Check for updates

View Article Online
View Journal

Catalysis
Science &
Technology

Accepted Manuscript

This article can be cited before page numbers have been issued, to do this please use: P. Carro, J. Choi, D. MacFarlane, A. N. Simonov, J. M. Doña-Rodriguez and L. M. Azofra, *Catal. Sci. Technol.*, 2022, DOI: 10.1039/D2CY00389A.

Catalysis
Science &
Technology

Volume 7
Number 2
21 January 2017
Pages 313-534

rsc.li/catalysis

ISSN 2044-4761

ROYAL SOCIETY
OF CHEMISTRY

PAPER
Chaoqiu Chen, Yong Qin *et al.*
Highly dispersed Pt nanoparticles supported on carbon nanotubes produced by atomic layer deposition for hydrogen generation from hydrolysis of ammonia borane

This is an Accepted Manuscript, which has been through the Royal Society of Chemistry peer review process and has been accepted for publication.

Accepted Manuscripts are published online shortly after acceptance, before technical editing, formatting and proof reading. Using this free service, authors can make their results available to the community, in citable form, before we publish the edited article. We will replace this Accepted Manuscript with the edited and formatted Advance Article as soon as it is available.

You can find more information about Accepted Manuscripts in the Information for Authors.

Please note that technical editing may introduce minor changes to the text and/or graphics, which may alter content. The journal's standard Terms & Conditions and the Ethical guidelines still apply. In no event shall the Royal Society of Chemistry be held responsible for any errors or omissions in this Accepted Manuscript or any consequences arising from the use of any information it contains.

ROYAL SOCIETY
OF CHEMISTRY

rsc.li/catalysis

View Article Online
DOI: 10.1039/D2CY00389A

ARTICLE

Competition between metal-catalysed electroreduction of dinitrogen, protons, and nitrogen oxides: a DFT perspective

Received XXth XXXX 2022,
Accepted XXth XXXX 2022

DOI: 10.1039/x0xx00000x

Pilar Carro,[a] Jaecheol Choi,[bc] Douglas R. MacFarlane,[bc] Alexandr N. Simonov,[bc]* José Miguel Doña-Rodríguez[d] and Luis Miguel Azofra[d]*

Production of green ammonia through electrochemical reduction of N_2 is amongst the major challenges of applied catalysis today. A large number of materials have been reported to be capable of catalysing the nitrogen reduction reaction (NRR), but the reliability of these results has been questioned due to the lack of evidence for N_2 being the source of produced NH_3. In the present study, we use density functional theory (DFT) to demonstrate that the NRR is highly unfavoured *versus* the hydrogen evolution reaction (HER) on a wide selection of metal catalysts, some of which have been reported to be active for the N_2 electroreduction to ammonia previously. Most importantly, we provide a comprehensive analysis of ammonia formation through electroreduction of nitrogen oxides, specifically NO and NO_2, which are very hard to avoid as impurities in the NRR experiments, and demonstrate that these processes can effectively compete with the HER. In general, N_2 weakly adsorbs on the metal surfaces but NO and NO_2 exhibit stronger interactions and a greater stability of the reduced intermediates. These results highlight NO/NO_2 reduction as a potential source of ammonia in NRR experiments and might also guide future design of catalysts for the fundamentally and practically important nitrogen oxide reduction reactions.

Introduction

The Haber–Bosch process[1] for ammonia synthesis through catalytic reduction of dinitrogen with hydrogen gas is still one of the most important technologies of the contemporary chemical industry,[2] but concerns about its sustainability call for the development of alternative methods to produce NH_3.[3] N_2 is one of the most stable molecules with a N≡N bond dissociation enthalpy of 946 kJ mol^{-1}, which explains the energy intensive conditions of the Haber–Bosch reaction that follows the so-called dissociative pathway (Fig. 1).[4–6] The rate-determining step (RDS) in this mechanism is dissociative chemisorption of N_2 on the catalytic metal surface. Once generated, adsorbed *N species react with adsorbed hydrogen atoms from H_2 eventually resulting in the production of NH_3.

In recent years, interest in electrochemical reduction of N_2 to NH_3 has substantially increased as an alternative to the Haber–Bosch process. When coupled to a suitable anode process, ideally the oxygen evolution reaction to extract electrons and protons from water, the nitrogen reduction reaction (NRR) can theoretically produce NH_3 at moderate temperatures (<100 °C) and pressures (<30 bar) while being powered by renewable electricity. Such a process, yet to be convincingly demonstrated in aqueous media, presents a broad range of advantages in terms of scalability and sustainability, and can be considered to produce genuinely "green" ammonia.[7] A plethora of materials has been claimed to be capable of catalysing the NRR in protic environments, majorly aqueous electrolyte solutions, but the reliability of most of these reports has been questioned.[8,9]

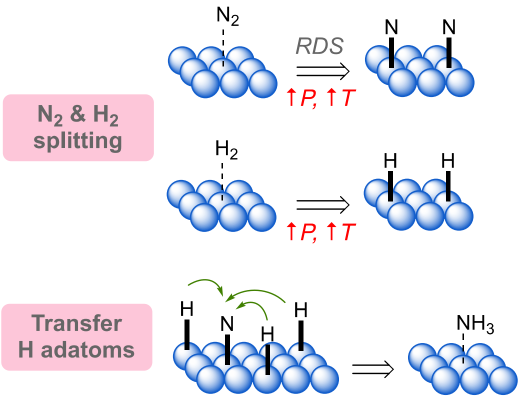

Figure 1. Dissociative mechanism of the Haber–Bosch process.[4–6]

The key experimental problem propagating through the field is the lack of control over nitrogenous compounds that are kinetically and thermodynamically much easier to reduce than N_2 on the ubiquitously applied metal electrodes, *viz.* nitrogen oxides like NO and NO_2.[10–12] Moreover, the majority of the

---

[a] *Área de Química Física, Departamento de Química, Facultad de Ciencias, Universidad de La Laguna, Instituto de Materiales y Nanotecnología. Avda. Francisco Sánchez, s/n, 38200 La Laguna, Tenerife, Spain.*
[b] *School of Chemistry, Monash University, Clayton, VIC 3800, Australia. E-mail: alexandr.simonov@monash.edu*
[c] *ARC Centre of Excellence for Electromaterials Science, School of Chemistry, Monash University, Clayton, VIC 3800, Australia.*
[d] *Instituto de Estudios Ambientales y Recursos Naturales (i-UNAT), Universidad de Las Palmas de Gran Canaria (ULPGC), Campus de Tafira, 35017 Las Palmas de Gran Canaria, Spain. E-mail: luismiguel.azofra@ulpgc.es*

†Electronic Supplementary Information (ESI) available: full computational details. See DOI: 10.1039/x0xx00000x

View Article Online
DOI: 10.1039/D2CY00080A

"successful" experimental NRR studies are commonly in direct conflict with the existing theoretical work. For example, different types of gold nanomaterials have been reported to be catalytically active for N_2 electroreduction[13–23] at potentials between –0.1 and –0.5 V *vs.* RHE (reversible hydrogen electrode), despite extreme thermodynamics difficulty of such process according to the density functional theory (DFT) analysis; specifically, Montoya *et al.*[24] calculated a value of *ca.* –3 V *vs.* CHE (computational hydrogen electrode) as the minimal potential required for N_2 electroreduction at the most stable Au(111) surface. A very similar value was also reported by Dražević and Skúlason.[25] In this context, bismuth presents another prominent example, for which an outstanding NRR catalytic performance at potentials between –0.6 and –0.8 V *vs.* RHE was reported.[26–28] However, the experimental values reported by Hao *et al.*[28] contradict their own theoretical results, which predict N_2 reduction to ammonia only at overpotentials in excess of 2.8 V on this metal.

The list of metals attempted for the N_2 electroreduction is long. Yet, while the metallic surfaces are often suggested as the active sites for the N_2 activation and reduction in such reports, these interpretations commonly ignore the marked nitrogen-phobic and hydrogen-philic nature of most metal surfaces. In other words, the hydrogen evolution reaction (HER) is a more preferred process, even with some of the worst HER catalysts such as bismuth and gold.[29]

The present work revisits the NRR *vs.* HER problem for a range of metallic surfaces, and most importantly, expands the previous DFT studies,[24,25,30–32] to include the competition with the reduction of nitrogen oxides (NO_x) —the likely source of ammonia in most aqueous N_2 electroreduction studies. In fact, the NO_x reduction reactions present both fundamental and practical interest on their own. Although the prospects of the conversion of NO_x to NH_3 are questionable from the agricultural perspective as plants preferably obtain N from the soil in the form of nitrate,[33] the NO_x to N_2 electroreduction has been long recognised as an important strategy to mitigate nitrogenous pollution in waterways.[34]

Results and discussion

H- *vs.* N_2H-philicity: The key to the HER *vs.* NRR selectivity. The direct electrocatalytic conversion of N_2 into two NH_3 molecules is a six-electron/six-proton process that can theoretically occur through the successive additions of the H^+/e^- pairs. In the framework of the proton coupled electron transfer (PCET) concept,[35] *i.e.*, when proton and electron reach the catalytic surface in a concerted way, the associative mechanism of the NRR starts with the adsorption of N_2 and the formation of the intermediate $^*N_2H$ species (* denotes adsorption on the catalyst surface):

$$^*N_2 + H^+ + e^- \rightleftarrows {}^*N_2H \qquad (1)$$

Similarly, the first step of the HER is the Volmer reaction producing a H adatom *via* reduction of H^+ on the catalyst surface as follows:

$$^* + H^+ + e^- \rightleftarrows {}^*H \qquad (2)$$

In the gas phase, a hypothetical $N_2(g) + H^+ + e^- \leftrightarrow N_2H(g)$ process presents an energy barrier amounting to –3.2 V *vs.* RHE,[36] but becomes much more energetically favourable upon the introduction of a catalyst. Fig. 2 presents the associative NRR pathway when it is assisted by the participation of a metal surface as an electrocatalyst. Once $^*N_2H$ is formed, the reaction proceeds to generate two molecules of NH_3 through steps comprising the $^*N{=}NH_2$, $^*N$, $^*NH$ and $^*NH_2$ intermediates, or alternatively, through $^*NHNH$, $^*NHNH_2$, $^*NH$, and $^*NH_2$. Note that the path towards hydrazine formation, NH_2NH_2, is mechanistically viable, but usually more energetically demanding.

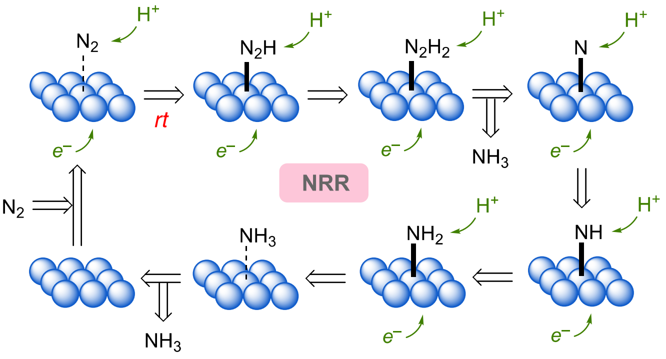

Figure 2. Associative pathway of the NRR catalysed by metal surfaces. "*rt*" means room temperature.

While a range of metals have been predicted by Skúlason *et al.*[30] to allow the associative NRR to occur at overpotentials ranging from 0.5 to 1.0 V, none of these have been unambiguously proven to be active catalysts through experiments. In fact, this is not entirely surprising, since the seminal and inspirational works by Skúlason *et al.*[25,30,32] predicted that the surface of most metals will be covered by H adatoms, rather than intermediates of the NRR, amongst other studies. Surprisingly, this important analysis of the competition between the NRR and HER is not usually adopted in many other computational works, which primarily focused on the analysis of reactive trends and rate-limiting steps for the N_2 reduction on its own. Considering this selectivity aspect, the field is yet to comprehensively address the question of the possibility of an electrocatalyst capable of suppressing the HER in favour of the NRR in protic media, with notable exceptions as those works recently reported by Singh, Rohr, and co-workers.[37,38]

Competition between the elementary steps in Eqns. (1) and (2) is one important aspect that affects the NRR *vs.* HER selectivity. For a given material, comparisons of the free energies of these reactions, *viz.* $\Delta G(^*N_2H)$ and $\Delta G(^*H)$ can allow

View Article Online
DOI: 10.1039/D2CY00089A

prediction of its specific behaviour with respect to electrocatalysis of the nitrogen reduction and hydrogen evolution reactions. These first reduction events might not be the RDS of the overall processes, but their interplay does determine the NRR *vs.* HER selectivity. In other words, if one of the reactants (N_2 or H^+) is preferentially reduced and the reduced species ($*N_2H$ or $*H$) dominate the active sites on the catalyst surface when an electrical potential (ε) is applied, the corresponding reduction reaction (NRR or HER) will be the dominant process in the system.

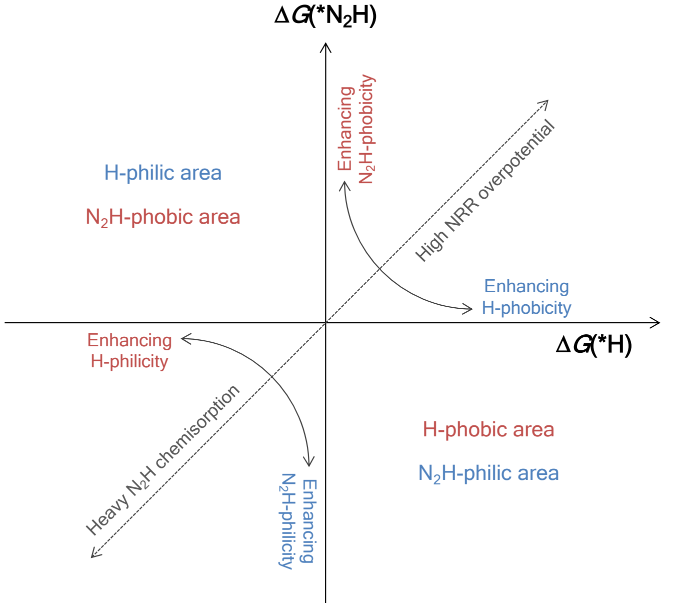

Figure 3. Prediction of the NRR *vs.* HER selectivity through the comparison of the free energies of the formation of $*N_2H$ and $*H$.

In terms of free energy, *i.e.*, $\Delta G = -nF\varepsilon$, the most favourable scenario for the N_2 reduction to occur corresponds to $\Delta G(*N_2H) < 0$ and $\Delta G(*H) > 0$ (fourth quadrant of Fig. 3). This requires that the material behaves as a H-phobic and N_2H-philic electrocatalyst that would promote the NRR but not the HER. On the contrary, if $\Delta G(*N_2H) > 0$ and $\Delta G(*H) < 0$ (the second quadrant, Fig 3), the surface is H-philic and N_2H-phobic, *i.e.*, H_2 will likely be produced in preference to NH_3. Theoretically, the material will be more selective towards the NRR than HER if $\Delta G(*N_2H) < \Delta G(*H)$. However, it is well understood from the Sabatier principle that both excessively positive and negative $\Delta G(*N_2H)$ values would be unfavourable for the N_2 reduction[39] irrespective of the competition with the H_2 evolution process.

To demonstrate the strategy based on the $\Delta G(*N_2H)$ *vs.* $\Delta G(*H)$ comparisons, we have analysed the binding properties of the N_2H and H species on a range of transition metals (*d*-block), namely: (i) fcc Ni, Cu, Rh, Pd, Ag, Ir, Pt, and Au; (ii) bcc V, Fe, Nb, and Mo; and (iii) hcp Ti, Co, Zn, Ru, Re, and Os. We have circumscribed our analysis to the flat (111), (110), and (001) facets for the fcc, bcc, and hcp lattices, respectively, since these facets have the highest planar density in the respective crystal structures. We have also included two metals from the *p*-block, namely Pb (fcc) and Bi (rhombohedral) with (111) and (001) surfaces, respectively.

The data is plotted in Figure 4 using the format of Figure 3. Immediately notable is the much wider range of $\Delta G(*N_2H)$ values (–2.8 to 2.9 eV) than is the case for $\Delta G(*H)$ (–1.0 to 1.0 eV). Except for the late transition metals Au, Ag, and Zn which behave as the *p*-block Pb and Bi metals (*red* symbols in Fig. 4), the formation free energies of $*N_2H$ and $*H$ correlate ($R^2 = 0.85$) for the other metals examined (*blue* symbols in Fig. 4). Thus, the greater the stabilisation of the $*N_2H$ species, the stronger the adsorption of the H adatom and *vice versa*. Au, Ag, and Zn and the *p*-block metals Pb and Bi show a limited affinity to N_2H with $\Delta G(*NH_2)$ values greater than 2 eV. In addition, $*H$ formation on these metals is also thermodynamically unfavourable although the corresponding free energies are less positive than $\Delta G(*N_2H)$. Metals from groups 7–10 and Cu belong to the N_2H-phobic and H-philic domain. Only the early transition metals Ti, V, Nb, and Mo exhibit $\Delta G(*N_2H) < \Delta G(*H)$ (*green* labels in Fig. 4). Thus, from a mechanistic point-of-view, only these metals amongst those examined can be theoretically expected to facilitate the highly selective reduction of N_2 into the adsorbed N_2H species rather than the reduction of protons into H-adatoms.

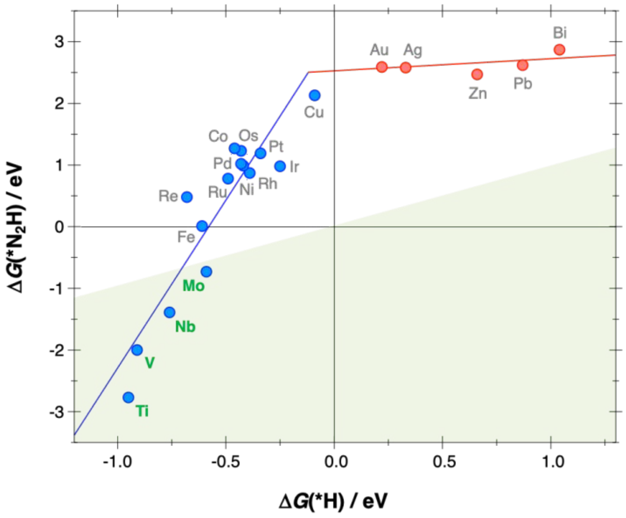

Figure 4. $\Delta G(*N_2H)$ *vs.* $\Delta G(*H)$ plot for the examined metals. Lines show linear fits for two distinct groups of metals. *Green* shaded area indicates where $\Delta G(*N_2H) < \Delta G(*H)$ and *green* labels highlight metals with where this is the case.

However, the hypothesis that the early transition metals Ti, V, Nb, and Mo might act as viable NRR catalysts is overshadowed by their oxyphilic nature and ensuing challenges with obtaining pure metallic surfaces under protic conditions. Possibly, this is one of the reasons for the lack of any convincing reports on the successful electrocatalysis of the N_2 reduction by these metals. In fact, rigorous investigation of Mo metal particles as catalysts for the NRR in both aqueous and aprotic electrolyte solutions demonstrated their very limited, if any, catalytic activity for the N_2 reduction to ammonia.[40]

Overall, the computational results presented here and elsewhere[25] confirm that the heterogeneous electrocatalysis of the direct N_2 reduction into NH_3 by metals presents a process of great difficulty that can be theoretically possible only on a very limited number of metallic surfaces.

Not only from the experimental perspective but also from the computational side, the community has recognised that the HER is not the only competing process in the NRR experiments. Of a specific concern is the reduction of nitrogen oxides —major air pollutants derived from industrial activity[41] and commonly present in N_2 gas. These processes can either produce dinitrogen or ammonia, *i.e.*, are a potential source of false-positive NRR results. This prompted us to investigate these processes following the approach discussed above.

The facile nitric oxide reduction reaction (NORR). The reduction of nitric oxide offers certain mechanistic advantages with respect to the NRR. First, the NORR is a five-electron process starting with the adsorption of NO to the reactive surface followed by the formation of the NOH intermediate species during the first H^+/e^- pair transfer. We have also considered the first hydrogenation of NO at the O atom leading to the ONH species, which however was found to be unstable intermediates (Fig. S4). It is also noted that the modelling of the NO adsorption on the surface of the selected metals through the O atom is less favourable than the adsorption *via* N (Fig. S4). In the second hydrogenation step, a water molecule is released producing the adsorbed *N (Fig. 5), which further transformations are the same as for the NRR (Fig. 3).

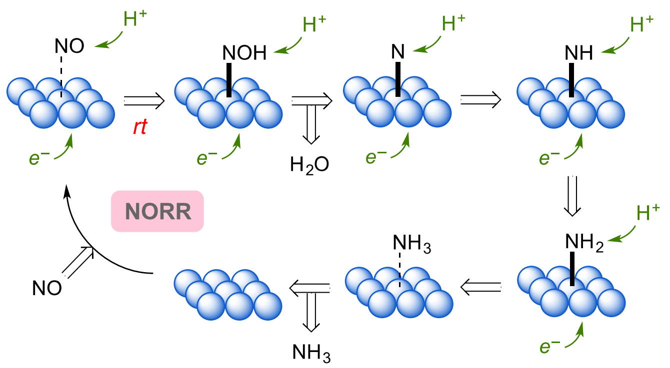

Figure 5. Associative pathway for the NORR catalysed by metal surfaces.

Contrary to N_2, a molecule presenting weak lone pairs on each nitrogen atom (:N≡N:), NO contains an unpaired electron on the N atom making it quite nucleophilic. Surface metal atoms behave as electropositive centres, thus metal···NO interactions are expected to be much stronger than the weak metal···N_2 bonds. This is one factor rendering the NORR a preferable process than the NRR, though similar predictions with respect to the HER require quantitative comparisons of the adsorption free energies of NO and H following the approach illustrated in Fig. 3. Similar to the ΔG(*N_2H) *vs.* ΔG(*H) pattern (Fig. 4), the ΔG(*NO) *vs.* ΔG(*H) plot revealed two distinct groups amongst the examined metals (Fig. 6). Again, Au, Ag, Zn, and the *p*-block metals Pb and Bi exhibit non-spontaneous NO adsorption [ΔG(*NO) between 0.14 and 0.34 eV] with no clear dependence on ΔG(*H) (*red* in Fig. 6), contrasting the direct correlation (R^2 = 0.92) between NO and H adsorption observed for the free energies of the *d*-metals (*blue* in Fig. 6).

In view of these results, it can be concluded that the capacity of the examined metals to stabilise the *N_2H intermediate of the NRR comes along with the strong affinity to bind *NO (inset to Fig. 6, R^2 = 0.85). Considering that the latter is always significantly more preferred [compare ΔG(*N_2H) in Fig. 4 and ΔG(*N_2H) in Fig. 6], the NORR is predicted to be always a dominant process as opposed to the NRR when nitric oxide is present in the system along with N_2.

There is also an essential difference in the catalytic behaviour of the NRR and NORR from the perspective of competition with the HER. While *H adsorption is preferred over *N_2H for the majority of the investigated metals (*green* labels in Fig. 4), the *NO binding is stronger than the adsorption of hydrogen for all examined surfaces except Au (*green* labels in Fig. 6). Mechanistically speaking, reduction of hydrogen will be substantially suppressed in presence of nitric oxide, which is expected to be the dominant adsorbed species on the active metal centres. In the case of Au, ΔG(*NO) is only slightly, by *ca* 0.05 eV, more positive than ΔG(*H), which indicates a Boltzmann population for the adsorbed hydrogen and nitric oxide species of 88:12. Hence, both HER and NORR might occur on the Au(111) surface with the former being the dominant process, although it is acknowledged that the calculated values are within the computational error.

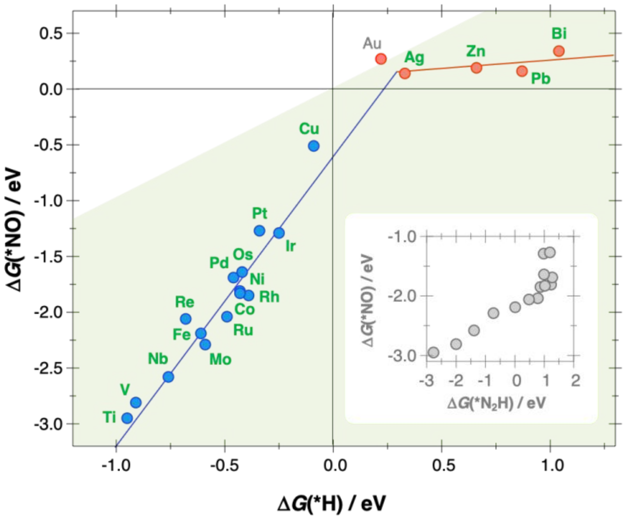

Figure 6. ΔG(*NO) *vs.* ΔG(*H) plot for the examined metals. Lines show linear fits for two distinct groups of metals. *Green* shaded area indicates where ΔG(*NO) < ΔG(*H) and *green* labels highlight metals with where this is the case. Inset shows the ΔG(*NO) *vs.* ΔG(*N_2H) plot for transition metals examined herein.

The theoretical predictions summarised above are consistent with our experimental studies on the carbon-supported Au nanoparticles used for the electroreduction of aqueous 0.5 M K_2SO_4 electrolyte solutions (pH = 3.5) saturated with N_2 and NO.[8] When tested for the NRR, no measurable activity of Au was detected and all reductive charge passed could be confidently ascribed to the HER. On the contrary, the Au-catalysed NO reduction commenced at potentials close to 0 V *vs.* RHE and produced NH_3 at *ca* 30% faradaic efficiency during chronopotentiometric tests at −0.30 V *vs.* RHE. It is noted that only NH_3 was quantified as the product of the NORR, *i.e.*, the remaining charge is consumed either in the HER or for the reduction on nitric oxide to other products like N_2.

The whole path for the NORR was analysed for all metals, with selected examples of free energy reaction profiles shown in Fig. 7, along with the optimised intermediate structures for the Cu(111) surface. Binding energy values for all intermediates along the NORR pathway, namely, *NO, *NOH, *N (plus H_2O release), *NH, $*NH_2$ and $*NH_3$ are also summarised in Table S3. In general, two common features for the investigated group of metallic models were established: (i) adsorption of NO occurs *via* the N atom; and (ii) the first hydrogenation step occurs through the O atom leading to the *NOH intermediate and never to the unstable *ONH species. See Fig. S3 for full details concerning the optimised structures for the HER, NRR, and NORR, as well as NO_2RR and N_2ORR, that will be discussed in upcoming sections.

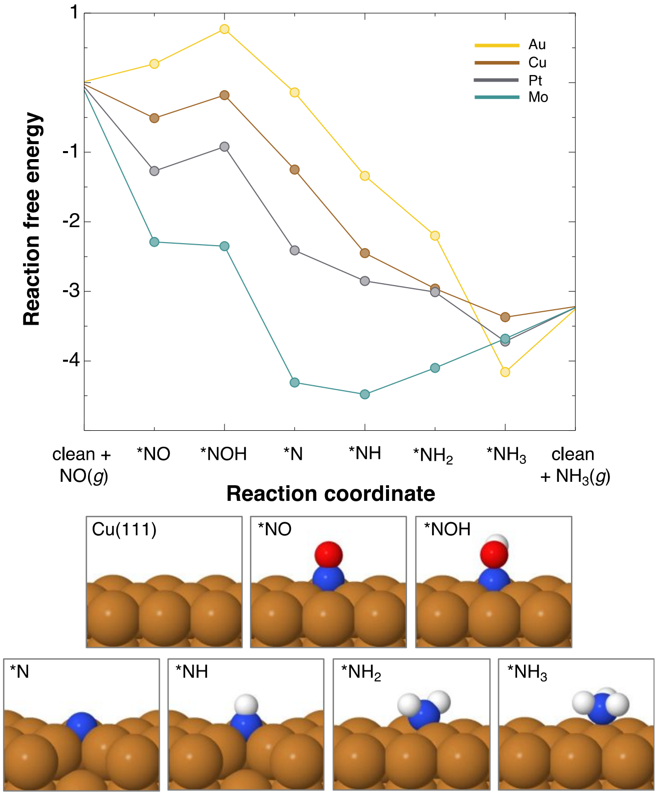

Figure 7. (a) The NORR energy profiles for Au, Cu, Pt and Mo. For the rest of the metals, see full free energy details in Table S3. Reaction free energies at room temperature are shown in eV. (b) Optimised structures for the case of the NORR catalysed by Cu(111).

Further, we extended the analysis of the NO reduction to understand the thermodynamics of the process towards the formation of ammonia. The adsorption free energy of the second intermediate of the NORR, *viz.* *NOH, was again found to correlate with Δ*G*(*H) (Fig. 8) in a manner that is qualitatively similar to that found for Δ*G*(*NO) (Fig. 6). However, the examined metals can be now classified into three groups.

First, early transition metals Ti, V, Nb, and Mo, along with Re and Os exhibit spontaneous values of NOH formation relative to NO. Second, these values are positive for late transition metals Au and Ag and the *p*-block metals Pb and Bi, specifically 0.50, 0.65, 0.48, and 0.85 eV, respectively, with Zn somewhat out of this trend of moderate non-spontaneous values (just 0.16 eV). Finally, NO to NOH is catalysed by Fe, Ru, Ir, Cu, Pt, Co, Rh, and Ni in a facile manner just demanding 0.13, 0.17, 0.18, 0.33, 0.35, 0.44, 0.44, and 0.51 eV, respectively (Pd is out of this trend with 0.73 eV).

Based on data at Table S3, theoretical reduction potentials of NO to NH_3, estimated as thermodynamics barriers, are between −0.16 and −0.85 V *vs.* CHE (computational hydrogen electrode) for the groups of metals selected in this study. In addition, Table S4 gathers the maximum energetic barriers, identifying the limiting step, as well as NH_3 desorption free energies required for the NORR in each metal. In this sense, formation of the NOH intermediate species is usually the RDS on most of the metals, although for others such as Fe, Nb, Ti, Ru, Re, and Os, the RDS is hypothesised to be the formation of the NH_2 species.

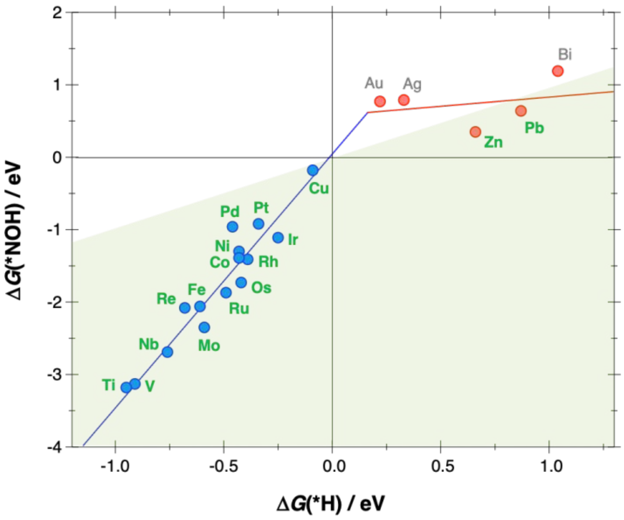

Figure 8. Δ*G*(*NOH) *vs.* Δ*G*(*H) plot for the examined metals. Lines show linear fits for two distinct groups of metals. *Green* shaded area indicates where Δ*G*(*NOH) < Δ*G*(*H) and *green* labels highlight metals with where this is the case.

Nitrogen dioxide reduction reaction (NO_2RR): A low energy process towards the formation of NO. Nitrogen dioxide, another common

View Article Online
DOI: 10.1039/D2CY00382A

nitrogenous pollutant,[42] was also analysed using the framework summarised in Fig. 3. The NO_2 reduction reaction (NO_2RR) is a seven-electron process in which the initial two hydrogenation steps of the adsorbed nitrogen dioxide produce $^*NO_2H$ and then $^*NO$ species, accompanied by a release of H_2O (Fig. 9). Exploration of the potential energy surfaces (PES) for the selected series of metals indicates that NO_2 binds with a bidentate configuration through its O atoms, however binding of the $^*NO_2H$ to the surfaces of the examined metals is more favourable through the N atom and hydrogenation occurs at one of the O atoms (Fig. 10). Upon completion of the two initial H^+/e^- transfer steps, a $^*NO$ intermediate is produced on the surface and further reduction occurs as in the NORR.

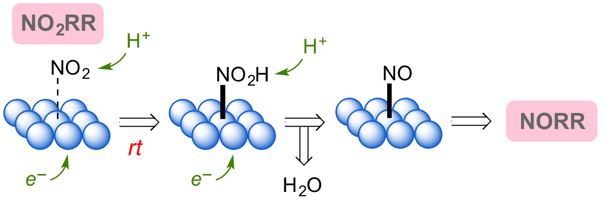

Figure 9. Associative pathway for the NO_2RR catalysed by metal surfaces.

A distinctive feature of the NO_2RR is that both $\Delta G(^*NO_2)$ and $\Delta G(^*NO_2H)$ are lower than $\Delta G(^*H)$ for all the studied metals (Fig. 11 and Table S3), indicating a preferential stabilisation of the initial intermediates of the nitrogen dioxide reduction rather than *H adatoms. Moreover, calculated $\Delta G(^*NO_2)$ and $\Delta G(^*NO_2H)$ were always negative, further suggesting that the initial steps of the NO_2RR will be dominant against the HER. Nevertheless, the qualitative pattern of the $\Delta G(^*NO_2)$ *vs.* $\Delta G(^*H)$ and $\Delta G(^*NO_2H)$ *vs.* $\Delta G(^*H)$ were similar to those discussed above for the NRR and NORR. Consequently, the $\Delta G(^*NO_2)$ *vs.* $\Delta G(^*N_2)$ plots exhibit a close to linear correlation, indicating that the metal surfaces that might theoretically bind N_2 will adsorb NO_2 even more strongly (Fig. 11a, inset, R^2 = 0.73). The only exception from this trend is titanium. It was found that NO_2 is not stabilised on the surface of this metal, and it is decomposed during optimisation.

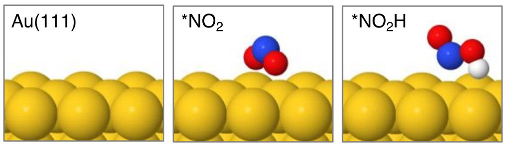

Figure 10. Optimised $^*NO_2$ and $^*NO_2H$ intermediate structures for the NO_2RR catalysed by Au(111).

Theoretical predictions of the facile electroreduction of NO_2 are also confirmed by our recent experimental studies of the bismuth powder material.[8] While being a poor catalyst for the nitrate reduction and essentially inactive for the NRR, Bi was found to effectively catalyse the reduction of electrolyte solutions purged with NO_2 with the formation of ammonia. It is noted that bismuth was calculated herein to exhibit the least favourable $\Delta G(^*NO_2)$ and $\Delta G(^*NO_2H)$ values (Fig. 11), suggesting that other metals examined would be even better catalysts for the NO_2RR.

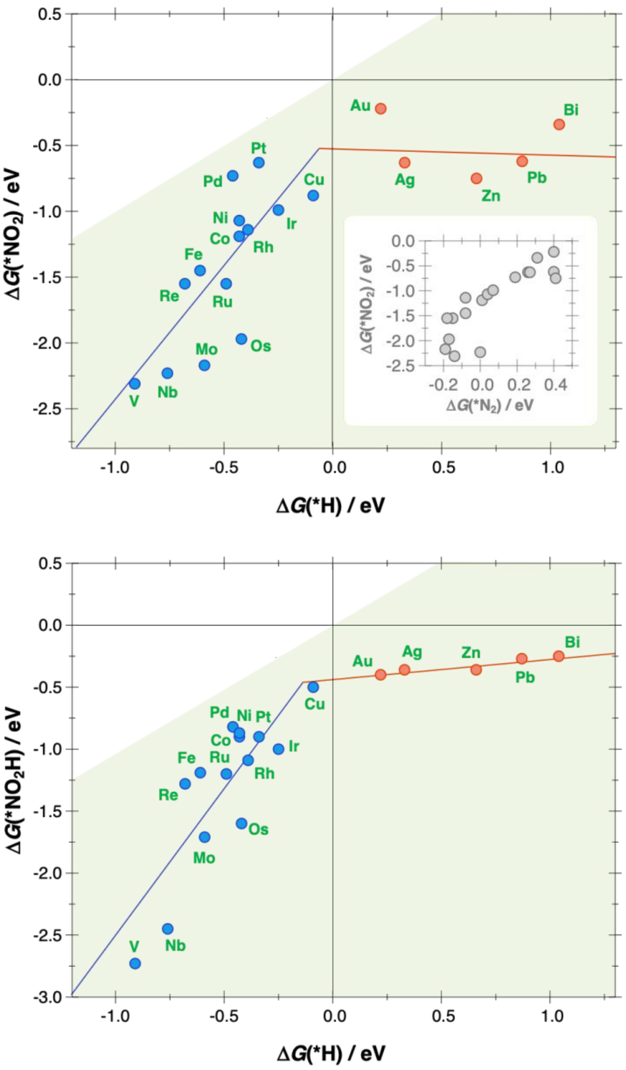

Figure 11. (a) $\Delta G(^*NO_2)$ *vs.* $\Delta G(^*H)$ and (b) $\Delta G(^*NO_2H)$ *vs.* $\Delta G(^*H)$ plots for the examined metals. Lines show linear fits for two distinct groups of metals. Inset in panel (a) shows the $\Delta G(^*NO_2)$ *vs.* $\Delta G(^*N_2)$ plot. *Green* shaded area indicates where (a) $\Delta G(^*NO) < \Delta G(^*H)$ and (b) $\Delta G(^*NOH) < \Delta G(^*H)$, and *green* labels highlight metals with where this is the case.

Nitrous oxide reduction reaction (N_2ORR): the least favourable of the NO_x reduction processes. Finally, the reduction of N_2O— a highly potent greenhouse gas emitted to the atmosphere through various anthropogenic pathways[43] — was investigated.

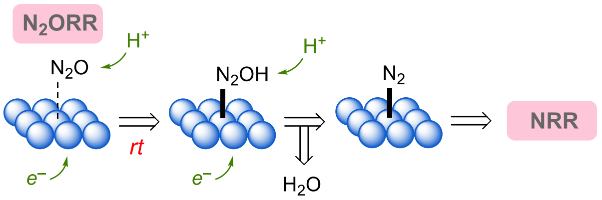

View Article Online
DOI: 10.1039/D2CY00589A

Figure 12. Associative pathway for the N_2ORR catalysed by metal surfaces.

Upon adsorption on the electrode surface, the $*N_2O$ moiety undergoes two successive H^+/e^- transfers that lead to the formation $*N_2OH$ (accompanied by a release of H_2O) and then $*N_2$ (Fig. 12). Thus, the N_2ORR to ammonia is an eight-electron process that can be considered as a two-electron process followed by the NRR.

Our DFT calculations reveal that N_2O interacts with the surfaces of examined metals weakly, *viz.* with positive $\Delta G(*N_2O)$ values in most cases (Fig. 13 and Table S3). Only the early transition metals Ti, Mo, and V show slightly negative binding energies within the –0.1 to –0.2 eV range. Again, binding of N_2O through the terminal N atom was energetically preferred to adsorption *via* the oxygen atom (Fig. S3). As has been common in all cases thus far, two groups of metals demonstrating different correlation between binding energy of N_2O and $\Delta G(*H)$ were identified: one includes Au, Ag, Zn and the *p*-block metals Pb and Bi with less pronounced dependence (*red* symbols in Fig. 13), and the rest showing a clear linear trend (*blue* symbols in Fig. 13, $R^2 = 0.72$). Only the most H-phobic metals, namely Zn, Pb and Bi, show values of $\Delta G(*N_2O) < \Delta G(*H)$ (*green* symbols in Fig. 13,). In general, most metals display a poor N_2O-philicity. Binding free energies of N_2O were found to correlate linearly ($R^2 = 0.89$) with those for N_2 (inset to Fig. 13), but in this case adsorption of the dinitrogen molecule was slightly preferred, which is an important distinction from the behaviour established for NO and NO_2 (Figs. 6 and 11a).

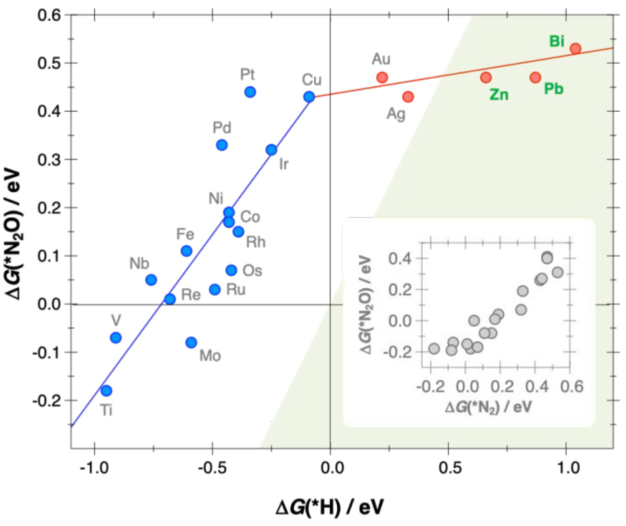

Figure 13. $\Delta G(*N_2O)$ *vs.* $\Delta G(*H)$ plot for the examined metals. Lines show linear fits for two distinct groups of metals. *Green* shaded area indicates where $\Delta G(*N_2O) < \Delta G(*H)$ and *green* labels highlight metals with where this is the case. Inset shows the $\Delta G(*N_2O)$ *vs.* $\Delta G(*N_2)$ plot for transition metals examined herein.

Moreover, analysis of the free energy for the formation of the $*N_2OH$ intermediate species produced $\Delta G(*N_2OH)$ values that were higher than the energy of *H adsorption in all cases except for Ti, V and Nb (Fig. 14). These three surfaces were predicted to promote decomposition of $*N_2OH$ intermediate into $*N_2$ and *OH moieties (captured on the surface) during optimisation.

Overall, all the data collectively suggest that electroreduction of N_2O is likely to be overrun by the H_2 evolution reaction and even the NRR, if the latter would be possible with the metals investigated herein.

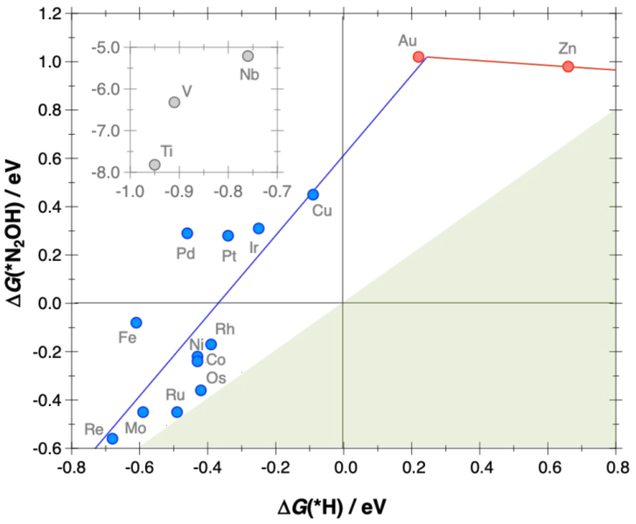

Figure 14. $\Delta G(*N_2OH)$ *vs.* $\Delta G(*H)$ plots for the examined metals. Lines show linear fits distinct groups of metals. *Green* shaded area indicates where $\Delta G(*N_2OH) < \Delta G(*H)$ and *green* labels highlight metals with where this is the case, *i.e.*, none in this case. Inset shows values for Ti, V and Nb, for which decomposition of $*N_2OH$ into $*N_2$ and *OH occurred during optimisation.

Conclusions

The electrochemical conversion of N_2 into NH_3 competes with the reduction of protons into H_2 in protic media. In general, the flat metal surfaces studied are more selective electrocatalysts for the HER, and those that are predicted to favour the NRR (Ti, V, Nb, and Mo) present a marked oxyphilic nature that prevents the obtaining of pure metallic surfaces under protic conditions. Our DFT observations emphasise the importance in the analysis of the N- *vs.* H-philic properties through the comparative analysis of the $\Delta G(*N_2H)$ and $\Delta G(*H)$ descriptors. These allow us to elucidate the selectivity of both processes. In general, most of the reported experimental studies employing metals as electrocatalysts are in direct contradiction with the theoretical results presented herein. We believe this can be explained by the reduction of adventitious NO_x species rather than N_2 in many published reports.

Indeed, the comprehensive DFT analysis presented herein demonstrates that NO and NO_2 reduction is preferred over the NRR and in some cases even over the HER for a wide range of metals. Importantly, the affinity of metal surfaces to the reductive adsorption of N_2 scales with the affinity to NO, NO_2 and N_2O. Moreover, while binding energies of N_2 and N_2O are generally very weak, NO and NO_2 are adsorbed strongly on most metals examined herein. Collectively this means that electroreduction of nitric oxide and nitrogen dioxide will be significantly preferable as compared to the reduction of dinitrogen. In other words, if NO_x contaminants are present, as is commonly the case even with the purified N_2 gas, they will be the first nitrogen-based species to be reduced.

Finally, we have also established a direct relationship between the H-philic and NO_x-philic properties, which are most pronounced for the transition *d*-metals and predicted that the NORR and NO_2RR are often energetically preferred processes over the reduction of protons into H_2. These results might support future developments of electrocatalytic systems for the NO_x reduction reactions under mild conditions.

Conflicts of interest

There are no conflicts to declare.

Acknowledgements

A.N.S. acknowledges the financial support by the Australian Research Council (DP200101878 and FT200100317). L.M.A. thanks the KAUST Supercomputing Laboratory using the supercomputer Shaheen II for providing the computational resources.

Notes and references

1 F. Haber and R. Le Rossignol, *Zeitschrift für Elektrochemie und Angew. Phys. Chemie*, 1913, **19**, 53–72.

2 V. Smil, *Nature*, 1999, **400**, 415.

3 D. R. MacFarlane, P. V Cherepanov, J. Choi, B. H. R. Suryanto, R. Y. Hodgetts, J. M. Bakker, F. M. Ferrero Vallana and A. N. Simonov, *Joule*, 2020, **4**, 1186–1205.

4 F. Bozso, G. Ertl, M. Grunze and M. Weiss, *J. Catal.*, 1977, **49**, 18–41.

5 F. Bozso, G. Ertl and M. Weiss, *J. Catal.*, 1977, 50, 519–529.

6 G. Ertl, S. B. Lee and M. Weiss, *Surf. Sci.*, 1982, **114**, 515–526.

7 D. R. MacFarlane, J. Choi, B. H. R. Suryanto, R. Jalili, M. Chatti, L. M. Azofra and A. N. Simonov, *Adv. Mater.*, 2020, **32**, 1904804.

8 J. Choi, H.-L. Du, C. K. Nguyen, B. H. R. Suryanto, A. N. Simonov and D. R. MacFarlane, *ACS Energy Lett.*, 2020, **5**, 2095–2097.

9 J. Choi, B. H. R. Suryanto, D. Wang, H.-L. Du, R. Y. Hodgetts, F. M. Ferrero Vallana, D. R. MacFarlane and A. N. Simonov, *Nat. Commun.*, 2020, **11**, 5546.

10 B. H. R. Suryanto, H.-L. Du, D. Wang, J. Chen, A. N. Simonov and D. R. MacFarlane, *Nat. Catal.*, 2019, **2**, 290–296.

11 S. Z. Andersen, V. Čolić, S. Yang, J. A. Schwalbe, A. C. Nielander, J. M. McEnaney, K. Enemark-Rasmussen, J. G. Baker, A. R. Singh, B. A. Rohr, M. J. Statt, S. J. Blair, S. Mezzavilla, J. Kibsgaard, P. C. K. Vesborg, M. Cargnello, S. F. Bent, T. F. Jaramillo, I. E. L. Stephens, J. K. Nørskov and I. Chorkendorff, *Nature*, 2019, **570**, 504–508.

12 A. J. Martín, F. L. P. Veenstra, J. Lüthi, R. Verel and J. Pérez-Ramírez, *Chem Catal.*, 2021, **1**, 1505–1518.

13 S.-J. Li, D. Bao, M.-M. Shi, B.-R. Wulan, J.-M. Yan and Q. Jiang, *Adv. Mater.*, 2017, **29**, 1700001.

14 M.-M. Shi, D. Bao, B.-R. Wulan, Y.-H. Li, Y.-F. Zhang, J.-M. Yan and Q. Jiang, *Adv. Mater.*, 2017, **29**, 1606550.

15 H. Ma, Z. Chen and Z. Wang, *Nanoscale*, 2021, **13**, 1717–1722.

16 J. Zheng, Y. Lyu, M. Qiao, J. P. Veder, R. D. Marco, J. Bradley, R. Wang, Y. Li, A. Huang, S. P. Jiang and S. Wang, *Angew. Chemie Int. Ed.*, 2019, **58**, 18604–18609.

17 Z.-H. Xue, S.-N. Zhang, Y.-X. Lin, H. Su, G.-Y. Zhai, J.-T. Han, Q.-Y. Yu, X.-H. Li, M. Antonietti and J.-S. Chen, *J. Am. Chem. Soc.*, 2019, **141**, 14976–14980.

18 L. Tan, N. Yang, X. Huang, L. Peng, C. Tong, M. Deng, X. Tang, L. Li, Q. Liao and Z. Wei, *Chem. Commun.*, 2019, **55**, 14482–14485.

19 J. Zhang, Y. Ji, P. Wang, Q. Shao, Y. Li and X. Huang, *Adv. Funct. Mater.*, 2020, **30**, 1906579.

20 D. Bao, Q. Zhang, F.-L. Meng, H.-X. Zhong, M.-M. Shi, Y. Zhang, J.-M. Yan, Q. Jiang and X.-B. Zhang, *Adv. Mater.*, 2017, **29**, 1604799.

21 M. Nazemi, S. R. Panikkanvalappil and M. A. El-Sayed, *Nano Energy*, 2018, **49**, 316–323.

22 Z. Wang, Y. Li, H. Yu, Y. Xu, H. Xue, X. Li, H. Wang and L. Wang, *ChemSusChem*, 2018, **11**, 3480–3485.

23 H. Wang, H. Yu, Z. Wang, Y. Li, Y. Xu, X. Li, H. Xue and L. Wang, *Small*, 2019, **15**, 1804769.

24 J. H. Montoya, C. Tsai, A. Vojvodic and J. K. Nørskov, *ChemSusChem*, 2015, **8**, 2180–2186.

25 E. Dražević and E. Skúlason, *iScience*, 2020, **23**, 101803.

26 L. Li, C. Tang, B. Xia, H. Jin, Y. Zheng and S.-Z. Qiao, *ACS Catal.*, 2019, **9**, 2902–2908.

27 Y. Wang, M. Shi, D. Bao, F. Meng, Q. Zhang, Y. Zhou, K. Liu, Y. Zhang, J. Wang, Z. Chen, D. Liu, Z. Jiang, M. Luo, L. Gu, Q. Zhang, X. Cao, Y. Yao, M. Shao, Y. Zhang, X.-B. Zhang, J. G. Chen, J. Yan and Q. Jiang, *Angew. Chemie Int. Ed.*, 2019, **58**, 9464–9469.

28 Y.-C. Hao, Y. Guo, L.-W. Chen, M. Shu, X.-Y. Wang, T.-A. Bu, W.-Y. Gao, N. Zhang, X. Su, X. Feng, J.-W. Zhou, B. Wang, C.-W. Hu, A.-X. Yin, R. Si, Y.-W. Zhang and C.-H. Yan, *Nat. Catal.*, 2019, **2**, 448–456.

29 S. Trasatti, *J. Electroanal. Chem. Interfacial Electrochem.*, 1972, **39**, 163–184.

30 E. Skúlason, T. Bligaard, S. Gudmundsdóttir, F. Studt, J. Rossmeisl, F. Abild-Pedersen, T. Vegge, H. Jónsson and J. K. Nørskov, *Phys. Chem. Chem. Phys.*, 2012, **14**, 1235–1245.

31 A. J. Medford, A. Vojvodic, J. S. Hummelshøj, J. Voss, F. Abild-Pedersen, F. Studt, T. Bligaard, A. Nilsson and J. K. Nørskov, *J. Catal.*, 2015, **328**, 36–42.

32 B. M. Ceballos, G. Pilania, K. P. Ramaiyan, A. Banerjee, C. Kreller and R. Mukundan, *Curr. Opin. Electrochem.*, 2021, **28**, 100723.

33 M. Sebilo, B. Mayer, B. Nicolardot, G. Pinay and A. Mariotti, *Proc. Natl. Acad. Sci.*, 2013, **110**, 18185–18189.

34 F. Gholami, M. Tomas, Z. Gholami and M. Vakili, *Sci. Total*

View Article Online
DOI: 10.1039/D2CY00389A

Environ., 2020, **714**, 136712.

35 S. Hammes-Schiffer, *Chem. Rev.*, 2010, **110**, 6937–6938.

36 C. J. M. van der Ham, M. T. M. Koper and D. G. H. Hetterscheid, *Chem. Soc. Rev.*, 2014, **43**, 5183–5191.

37 A. R. Singh, B. A. Rohr, J. A. Schwalbe, M. Cargnello, K. Chan, T. F. Jaramillo, I. Chorkendorff and J. K. Nørskov, *ACS Catal.*, 2017, **7**, 706–709.

38 A. R. Singh, B. A. Rohr, M. J. Statt, J. A. Schwalbe, M. Cargnello and J. K. Nørskov, *ACS Catal.*, 2019, **9**, 8316–8324.

39 H. Ooka, J. Huang and K. S. Exner, *Front. Energy Res.*, , DOI:10.3389/fenrg.2021.654460.

40 H.-L. Du, R. Y. Hodgetts, M. Chatti, C. K. Nguyen, D. R. Macfarlane and A. N. Simonov, *J. Electrochem. Soc.*, 2020, **167**, 146507.

41 J. Long, S. Chen, Y. Zhang, C. Guo, X. Fu, D. Deng and J. Xiao, *Angew. Chemie Int. Ed.*, 2020, **59**, 9711–9718.

42 P. Y. Oikawa, C. Ge, J. Wang, J. R. Eberwein, L. L. Liang, L. A. Allsman, D. A. Grantz and G. D. Jenerette, *Nat. Commun.*, 2015, **6**, 8753.

43 A. R. Ravishankara, J. S. Daniel and R. W. Portmann, *Science (80-.).*, 2009, **326**, 123–125.